Proceedings of *RAGtime 17–19*, 17–19/23–26 Oct., 1–5 Nov., 2015/2016/2017, *Opava, Czech Republic*
Z. Stuchlík, G. Török and V. Karas, editors, Silesian University in Opava, 2017, pp. 47–59

47

Epicyclic oscillations of thick relativistic disks

Jiří Horák [1], Odelle Straub [2], Eva Šrámková [3],
Kateřina Goluchová [3] and Gabriel Török [3]

[1]Astronomical Institute, Academy of Sciences,
  Boční II 141 31 Prague, Czech Republic
[2]LUTH, Observatoire de Paris, CNRS UMR 8102,
  Universite Paris-Diderot, 5 place Jules Janssen, F-92195 Meudon, France
[3]Institute of Physics, Silesian University in Opava,
  Bezručovo nám. 13, CZ-746 01 Opava, Czech Republic

ABSTRACT
We study epicyclic oscillations of thick relativistic tori with constant specific angular
momentum distribution using the finite element numerical method. We have com-
pared frequencies of the axisymmetric and non-axisymmetric modes with the ana-
lytic formulae obtained by Straub and Šrámková (2009) and Fragile et al. (2016). We
have found excellent agreement in the case of axisymmetric radial epicyclic modes.
In the case of the axisymmetric vertical epicyclic modes and non-axisymmetric
modes in general, the analytic approximation agrees with numerical results only for
tori of moderate thicknesses. Our analysis also revealed an instability of the thick
constant angular momentum tori with respect to the radial epicyclic oscillations.

Keywords: black hole physics – accretion disks – oscillations – FEM method

1 INTRODUCTION

A short-period variability of accreting neutron stars and black holes has motivated many
studies of oscillation properties of relativistic flows. Because a detailed geometry of ac-
cretion is not yet well understood, the most works concentrate either on oscillations of
Keplerian razor-thin disk-like flows or on geometrically thick toroidal flows of toroidal
shape, whose angular momentum profiles differ significantly from the Keplerian distribu-
tion. Although simple models of thick tori are known to be dynamically unstable to global
non-axisymmetric perturbation (Papaloizou and Pringle, 1984) and perhaps also locally
unstable, due to the magneto-rotational instability (Wielgus et al., 2015), they are often
used as first approximations of hot thick parts of accretion flows. In the truncated disk
scenario (Done et al., 2007), the outer thin disk is truncated at larger radii and the inner
part of the accretion flow has a form of geometrically thick flow. Numerical simulations of
the radiatively inefficient flow also often produce flow of substantial geometrical thickness
and significantly sub-Keplerian specific angular momentum distributions. These features
point to a significant pressure support, just as in the case of simple thick disk models and

perhaps also oscillations of these flows share many properties. In this context, the oscillations of thick disks still remains an active field of research. For example, Rezzolla et al. (2003) and Montero et al. (2004) studied radial axisymmetric oscillations in vertically integrated thick disks. Abramowicz et al. (2006) pointed out the existence of global epicyclic modes in relativistic slender tori. Their work was followed by Blaes et al. (2006), who presented a complete analysis of slender tori modes. Straub and Šrámková (2009) studied properties of the epicyclic modes in thicker tori using the perturbation expansion in the torus thickness around the slender torus limit. Recently, minor errors in their analysis were corrected subsequently by Fragile et al. (2016), who used their results to understand both a high-frequency and low-frequency variability of accreting black-hole GRO J1655-40.

In this note, we show that these considerations should be taken with some care. Our main finding is that tori of sufficient thickness are unstable with respect to the non-axisymmetric radial epicyclic oscillations. We also compare the analytical results of Fragile et al. (2016) with direct numerical solutions of the torus-oscillation problem. The plan of the paper is as follows. In section 2, we summarize the most relevant aspects of the theory of relativistic stationary thick disks relevant to our work. Section 3 contain a brief introduction the problem of thick disk oscillations, including some relevant mathematical results. Our numerical method is introduced in section 4. The results for axisymmetric and non-axisymmetric epicyclic modes are presented in sections 5 and 6, respectively. The section 7 discuss the mechanism of the instability and finally, section 8 is devoted to our conclusions.

2 EQUILIBRIUM

The equilibrium disk model corresponds to a relativistic torus orbiting a compact object in a stationary axially-symmetric spacetime. The complete analytic description of these solutions has been given by Abramowicz et al. (1978), (see also Kozlowski et al., 1978). The symmetries of the spacetime are described by two Killing vectors, t^μ (corresponding to stationarity) and ϕ^ν (corresponding to axial symmetry).

The matter forming the torus is described by the stress-energy tensor of ideal fluid,

$$T^\alpha_\beta = (e + p)u^\alpha u_\beta + p\delta^\alpha_\beta, \tag{1}$$

where e and p are the total energy density (including both, the rest-mass density and the internal energy) and pressure measured in the rest frame of the fluid. In the equilibrium, the four-velocity of the flow u^μ corresponds to a pure rotation,

$$u^\mu = A\left(t^\mu + \Omega\phi^\mu\right), \tag{2}$$

where $\Omega = \mathrm{d}\phi/\mathrm{d}t$ is the angular velocity of the flow measured at infinity and A is the redshift factor, a normalization constant following from the condition $u^\nu u_\nu = -1$. As already mentioned, we consider only tori with constant specific angular momentum ℓ. Therefore, we have

$$\Omega = \frac{g^{\phi t} - \ell g^{\phi\phi}}{g^{tt} - \ell g^{t\phi}}, \quad \ell \equiv -\frac{(u_\nu\phi^\nu)}{(u_\nu t^\nu)} = \text{const}, \tag{3}$$

where $g^{\mu\nu}$ denote contravariant components of the metric tensor.

◄◄ ◄ ► ►◄

The dynamics of the flow follows from the relativistic conservation laws; the Euler equation and the continuity equation,

$$\nabla_\alpha (\rho u^\alpha) = 0, \quad \nabla_\alpha T^\alpha_\beta = 0 \tag{4}$$

with ρ being the rest-mass density (e.g. particle number density multiplied by mass of a single particle). In our case, the continuity equation is satisfied trivially by the assumed symmetries of the flow and the nontrivial component of the Euler euqation gives

$$(e + p)\boldsymbol{a} + \boldsymbol{\nabla} p = 0, \quad \boldsymbol{a} = \boldsymbol{\nabla} \ln E \tag{5}$$

with $\boldsymbol{a}$ being a poloidal part of the four-acceleration and

$$E \equiv -u_\nu t^\nu = (-g^{tt} + 2\ell g^{t\phi} - \ell^2 g^{\phi\phi})^{-1/2} \tag{6}$$

being a sum of the kinetic and gravitational energies. In the case of adiabatic flows, $p = p(e)$ and $\Omega = \Omega(\ell)$, the equation (5) can be integrated to

$$Eh = \text{const}, \quad h \equiv \frac{e + p}{\rho}, \tag{7}$$

where h is the enthalpy. We restrict ourselves to the polytropic equation of state,

$$e = \rho + np, \quad p = K\rho^{1+1/n}, \tag{8}$$

where K and n are the polytropic constant and index. Surfaces of constant density and pressure coincide with surfaces of constant E ('equipotential' surfaces). As can be seen from equation (5), the equatorial circle $r = \text{const} \equiv r_0$ of the maximal pressure ('main circle' or the 'center' of the torus, r being the circumferential radius) corresponds to the geodesic. The flow rotates with Keplerian angular momentum at this radius. Inside/outside this radius, the motion is accelerated by the pressure gradient leading to super-/sub-Keplerian rotation. The location of the torus boundary (the equipotential with $p = 0$) depends on the parameter β, first introduced by Abramowicz et al. (2006),

$$\beta \equiv \frac{\sqrt{2n}c_{s0}}{A_0 r_0 \Omega_0}, \quad 0 < \beta < \beta_{\max}, \tag{9}$$

where c_{s0} is the local sound speed and the subscript '0' denotes an evaluation of the corresponding quantity at the torus center. This parameter roughly describes a ratio of the radial extend of the torus to the main-circle radius r_0 and will be further referred to as the thickness parameter. The lower limit $\beta \to 0$ corresponds to slender tori with small extend whose equipotential have elliptical cross-sections (Abramowicz et al., 2006). The upper bound $\beta_{\max}$ is determined by the maximal closed equipotential surrounding the main circle. This euipotential corresponds either to the self-crossing surface (in that case, the torus has a finite extend and terminates by the cusp at its inner edge) or to an open surface of the quasi-parabolic shape (in that case the torus outer edge is at infinity). The first case occurs in tori with centers located close to the compact object, the latter limits the torus sizes farther away. Fig. 1 shows few examples of these maximal configurations in Kerr spacetimes.
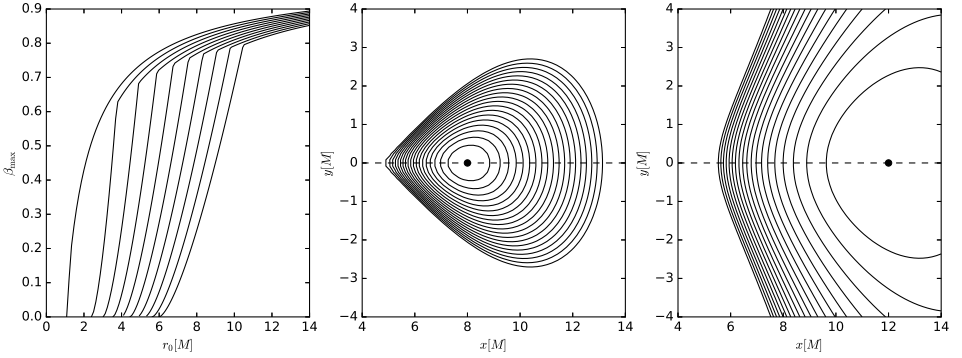
Figure 1. .Left: The upper bound on the torus thickness parameter $\beta_{\max}$ as a function of its main-circle radius r_0 for different black-hole spins (the curves from the right to left correspond to $a = 0, 0.1, 0.2, .., 0.9$ and 1). The polytropic index of the fluid is $n = 3$. The size of the torus is limited either by self-crossing equipotential surface or by first quasi-parabolical surface that opens to infinity. The first case corresponds to the initial steeper part of the $\beta_{\max}(r_0)$-curves closer to the black hole, the second case corresponds to the subsequent moderate growth farther away. Middle and right panels show examples of the two maximal configurations: torus terminated by the cusp for $a = 0$, $r_0 = 8M$ (middle) and an infinite torus for $a = 0$, $r_0 = 12M$ (right).

3 PERTURBATIONS

Due to the symmetries of the stationary configuration, a general linear perturbation of the torus can be decomposed into normal modes, whose dependence on time and azimuth is of the form of $\exp[i(m\phi - \omega t)]$ with m being an integer azimuthal wavenumber and ω is the oscillation frequency (eigenfrequency) of the mode as measured by a distant observer. Papaloizou and Pringle (1984) introduced a perturbation variable W to describe the spatial shape of the perturbations. Later on, its relativistic version has been introduced by Abramowicz et al. (2006) (see also Blaes et al., 2006)

$$W \equiv -\frac{\delta h}{\tilde{\omega}}, \tag{10}$$

where $\tilde{\omega} = A(\omega - m\Omega)$ is the frequency of oscillations measured in the comoving frame of the fluid. Perturbations of other quantities follow from W using

$$\delta \boldsymbol{u} = \frac{\mathrm{i}}{h}\boldsymbol{\nabla}W, \quad \delta u_t = \frac{\tilde{m}A}{\Omega h}W, \quad \delta u_\phi = -\frac{\tilde{m}A}{h}W, \quad \delta p = -\rho\tilde{\omega}W, \tag{11}$$

where $\tilde{m} = E(m - \ell\omega)$ and, again, boldface letters denote components of four-vectors in the poloidal plane $t = $ const, $\phi = $ const. The variable W is governed by the relativistic Papaloizou-Pringle equation

$$\frac{h}{\rho R}\boldsymbol{\nabla} \cdot \left(\frac{\rho R}{h}\boldsymbol{\nabla}W\right) + \left[\frac{\tilde{\omega}^2}{c_s^2} - \frac{\tilde{m}^2}{R^2}\right]W = 0, \tag{12}$$

where $R \equiv [(t_\nu\phi^\nu)^2 - (t_\nu t^\nu)(\phi_\nu\phi^\nu)]^{1/2} = (g_{t\phi}^2 - g_{tt}g_{\phi\phi})^{1/2}$. The equation (12), apart of some errors, has been first derived by Abramowicz et al. (2006). The boundary condition is that

of the free surface (i.e. vanishing Lagrangian pressure variation at the torus boundary). In terms of W, it is enough to demand W to be finite at the torus boundary.

Mathematically, the equation (12) represents a quadratic eigenvalue problem. To see it more explicitly, we can rewrite it as

$$\hat{L}W + (\omega - m\Omega_1)(\omega - m\Omega_2)W = 0, \tag{13}$$

where

$$\hat{L} \equiv \frac{h}{\rho R \mathcal{B}} \boldsymbol{\nabla} \cdot \left(\frac{\rho R}{h} \boldsymbol{\nabla}\right), \quad \mathcal{B} \equiv \frac{A^2}{c_s^2} - \frac{E^2 \ell^2}{R^2}, \quad \Omega_{1,2} \equiv \frac{AR\Omega \pm c_s E}{AR \pm c_s E\ell}. \tag{14}$$

Both, Ω_1 and Ω_2 tend to the rotational frequency Ω in the limit of vanishing sound speed. For a given value of the azimuthal wavenumber m, there is a set of discrete frequencies and eigenfunctions $\{\omega_n, W_n(\boldsymbol{x})\}$ that satisfy equation (13) with the boundary condition describing various modes of torus oscillations.

Consider now two functions U and V defined on the torus poloidal cross-section S and finite at its boundary ∂S. One may show that the operator $\hat{L}$ is self-adjoint with respect to the scalar product

$$\langle U|V \rangle \equiv \int_S U(\boldsymbol{x})V(\boldsymbol{x})w(\boldsymbol{x})\mathrm{d}S, \quad w(\boldsymbol{x}) = \frac{\rho R \mathcal{B}}{h}. \tag{15}$$

In the limit of slender tori, $\beta \to 0$, $\Omega_1 \approx \Omega_2 \approx \Omega_0$, the equation (13) becomes a linear self-adjoint eigenvalue problem with $\sigma^2 = (\omega - m\Omega_0)^2$ being the eigenvalue. Because the operator $\hat{L}$ is self-adjoint, it follows that its eigenvalues σ^2 are real and the corresponding eigenfunctions $W_n(\boldsymbol{x})$ form a complete orthogonal set.

Blaes et al. (2006) obtained analytic formulae describing lowest-order oscillation modes of relativistic slender tori. They also realized that due to a convenient structure of the operator $\hat{L}$ in this limit, the eigenfunctions are given by polynomials of finite order in the poloidal coordinates. In particular, the linear eigenfunctions correspond to the epicyclic modes. Later on, Straub and Šrámková (2009) studied the epicyclic modes in thicker tori (described by small but finite β) using perturbation expansion in the thickness parameter β. They expanded the eigenfunctions of a thicker torus in the basis of eigenfunctions of slender torus and found corrections due to a finite torus thickness to be

$$\omega_r = \omega_r^{(0)} + \beta^2 \omega_r^{(2)} + O(\beta^3), \quad W_r = W_r^{(0)} + \beta W_r^{(1)} + O(\beta^2) \tag{16}$$

and

$$\omega_v = \omega_v^{(0)} + \beta^2 \omega_v^{(2)} + O(\beta^3), \quad W_v = W_v^{(0)} + \beta W_v^{(1)} + O(\beta^2). \tag{17}$$

The leading-order correction $\omega_i^{(2)}$ and $W_i^{(1)}(\boldsymbol{x})$ are of the second order in the eigenfrequencies and of the first order in the eigenfunctions. They are given by the location of the pressure maximum r_0 and polytropic index n. The zeroth-order eigenfrequencies read $\omega_r^{(0)} = \omega_r + m\Omega_0$ and $\omega_v^{(0)} = \omega_\theta + m\Omega_0$, where ω_r and ω_θ are just radial and vertical geodesic epicyclic frequency, respectively. The Straub and Šrámková (2009) solution describes well a qualitative behavior of the epicyclic modes, nevertheless it was based on the Abramowicz et al. (2006) form of the Papaloizou-Pringle equation that contained few errors. The problem has been recently revisited by Fragile et al. (2016), who used a correct form of the Papaloizou-Pringle equation, and whose analytical results are used here.
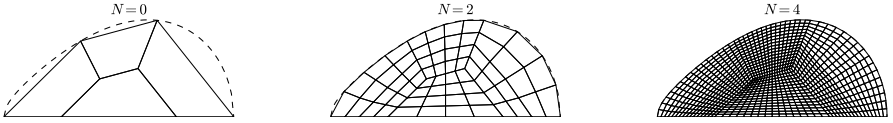
Figure 2. Quadrilateral triangulations covering the upper half of the torus cross-section used in the calculations. The initial ($N = 0$) triangulation is shown on the left, triangulations after $N = 2$ and $N = 4$ global refinements are shown in the middle and on the right, respectively. The number of the quadrilaterals after N global refinements is 4^{N+1}. The dashed line denotes the surface of the torus.

4   NUMERICAL CALCULATIONS

In this note, we use the finite elements method (FEM) to solve equation (13). By introducing an additional solution variable $\tilde{W} \equiv (\omega - m\Omega_1)W$, the quadratic eigenvalue problem is reduced to the linear one for a two-component solution vector $[W(\boldsymbol{x}), \tilde{W}(\boldsymbol{x})]$. We then find a weak form of the problem that is further discretized by expanding the solution in a finite set of suitable chosen shape functions (finite elements). This way the problem is finally reduced to an eigenvalue problem of a large sparse matrix.

Our implementation of FEM is based on the C++ library deal.II (Arndt et al., 2017). It uses a quadrilateral solution mesh ('quadrilateral triangulation'). We take advance of the equatorial plane symmetry of the stationary flow and solve the Papaloizou-Pringle equation in the upper half of the torus only. In the equatorial plane we impose additional boundary condition $W = 0$ or $\boldsymbol{n} \cdot \boldsymbol{\nabla} W = 0$ ($\boldsymbol{n}$ is a normal vector to the equatorial plane) according to the parity of the modes. Initially, we start with the triangulation consisting of 4 quadrilateral cells roughly resembling overall shape of the torus cross-section. The initial mesh is then N-times refined globally. In each refinement step, every cell is divided into four smaller cells, so the total number of quadrilaterals after N refinements is 4^{N+1} (see Fig. 2). We use standard scalar Lagrange finite elements Qp for both W and $\tilde{W}$ components. This yields a solution in terms of piecewise polynomials of the order of p. In this note we the simplest elements corresponding to $p = 1$. Indeed, using higher values of p would reduce a total number of cells needed to obtain the same accuracy of approximations, however at the same time it would increase the number of degree of freedoms per cell. The matrix eigenvalue problem is solved with the aid of the numerical library ARPACK. When the solution is obtained, its error is estimated by taking one more refinement step and comparing the new eigenfrequency with the previous one. We have tested this procedure on the case of very slender torus, where the eigenfunctions and eigenfrequencies are given by analytic expressions Blaes et al. (2006). Generally, we have found that the mashes of the order of $N = 2$ or 3 are sufficient for determination of eigenfrequencies of the epicyclic modes with precision better then 1%.

When examining the oscillation modes in thick tori, we assume that their eigenfrequencies and eigenfunctions are continuous functions of torus thickness. We trace the eigenfunctions of epicyclic modes in thick tori by starting at given radius with a slender torus and searching for a modes whose eigenfrequency is closest to the local epicyclic frequencies. We also check whether the corresponding eigenfunctions agree with Blaes et al. (2006) an-

alytic formula. We then gradually increase the thickness parameter β of the torus by steps $\Delta\beta$. In the $(i+1)$-th step we first select few (10) closest eigenfrequencies to the one obtained in the previous step (ω_i). For these modes, we map the corresponding eigenfunctions to the cross-section of the torus dealt with in the previous (i-th) step and calculate its correlation with the eigenfunction found in the i-th step. Finally, we chose the mode with the highest correlation. If no candidate mode gives acceptable correlation, we reduce the step size $\Delta\beta$ and repeat the procedure. Practically, we set the lower limit of acceptable correlation to 0.99. A typical step-size corresponding to this limit is $\Delta\beta = 0.01$. We trace the epicyclic modes over full range of $0 < \beta < \beta_{max}$ at various radii. This way we build up a grid covering all possible radii and thicknesses. The eigenfrequencies corresponding to a torus of a given r_0 and β are then found by an interpolation over this grid.

Although our numerical calculation is suitable for a general axisymmetric spacetime, in this note, we further restrict ourselves to relativistic tori around Kerr black holes. We also set the polytropic index to $n = 3$, what corresponds to radiation-pressure dominated flows.

5 AXISYMMETRIC EPICYCLIC MODES

Figure 3 shows behavior of the eigenfrequencies of the radial and vertical axisymmetric ($m = 0$) epicyclic modes with changing thickness parameter β. Each line corresponds to a given spin of the black hole and position of the torus center r_0 and traces the eigenfrequency over a full range of the thickness parameter. Therefore their endpoints thus correspond either to infinite tori or to finite tori with cusps at their inner edges. In the latter case, the eigenfrequencies vanishes as $\beta \to \beta_{max}$, because a torus center of the mass gradually moves to large radii. The analytic approximation based on Fragile et al. (2016) calculations are shown by dashed lines for comparison. In the case of the radial axisymmetric epicyclic mode, the second-order analytic predictions and the numerical calculations are in excellent agreement. On the other hand, use the analytic approximation for the vertical mode is rather limited to $\beta \lesssim 0.1$.

Figure 4 shows poloidal velocity fields corresponding to the two epicyclic modes in the cusp tori around Schwarzschild black hole, whose center is located at $r_0 = 9M$. We plot the contravariant components of the four-velocity in the Boyer-Lindquist coordinates calculated using equation (11). As can be seen from these relations, the four-velocity has also very small azimuthal component of purely relativistic origin, because $\tilde{m}$ does not vanish even for axisymmetric modes. The velocity patterns corresponding to epicyclic oscillations of thick tori differ substantially from uniform velocity fields found in slender tori. The oscillations take place mostly in outermost parts of the torus, while close to the cusp, the matter is practically unaffected.

6 NON-AXISYMMETRIC MODES

To explore properties of non-axisymmetric epicyclic modes, we concentrate on the $m = 1$ case. Since the equation (13) remains unchanged under the transformation $\omega \to -\omega$, $m \to -m$, all the results presented in this section can be applied to the case $m = -1$ as well. In slender tori, the eigenfrequencies of the non-axisymmetric oscillation modes are given by
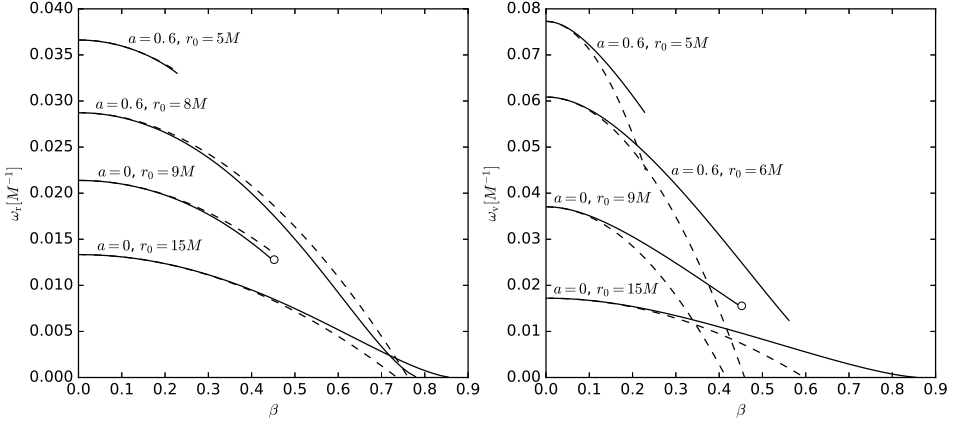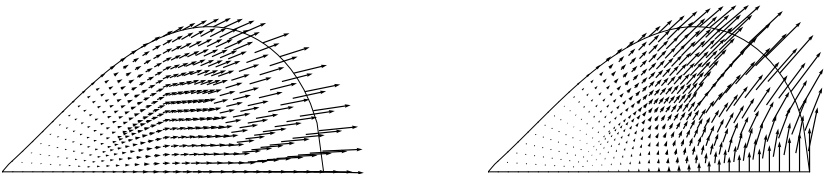
Figure 3. Eigenfrequencies of the radial (left) and vertical (right) epicyclic modes in relativistic tori surrounding Kerr black hole. The dashed lines show the analytical approximation of Fragile et al. (2016). The solid lines denote the numerical solutions of the equation (13). Each line corresponds to a sequence of tori with constant main-circle radius r_0 and changing thickness parameter β in a full range, $0 < \beta < \beta_{\mathrm{max}}$. The polytropic index is set to $n = 3$. The lines terminating at nonzero frequencies correspond to sequences terminating with a cusp torus. The circle indicates the solutions shown in Fig. 4.

Figure 4. Eigenfunctions of the radial (left) and vertical (right) epicyclic modes of relativistic tori with cusp surrounding Schwarzschild black hole. The arrows show contravariant Boyer-Lindquist components of the local velocity δv^i calculated using equation (11). The parameters of the torus are $r_0 = 9M$, $\beta = 0.452$ and $n = 3$ in both cases and correposond to the solutions indicated in Fig. 3 by the circle.
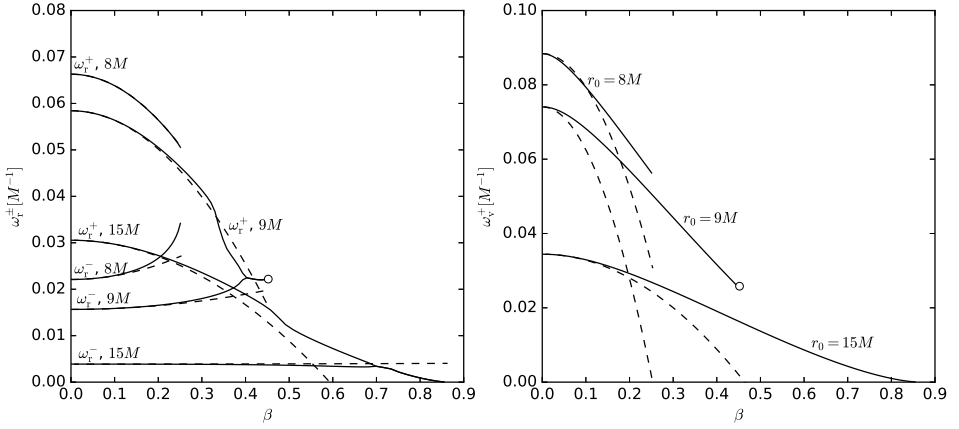
Figure 5. Eigenfrequencies of the non-axisymmetric ($m = 1$) radial and vertical epicyclic modes in relativistic tori surrounding Schwarzschild black hole at $r_0 = 8M, 9M$ and $15M$. Meaning of the lines is the same as in Fig. 3. In the case of radial modes (left), we show both, the r$^+$ and r$^-$ modes. If the torus is located sufficiently far away from the black hole (here the case of $r_0 = 9M$ and $15M$), the two radial epicyclic modes merge and create a couple of an overstable and damped mode. In the case of vertical modes (right), we show only the ω_v^+-mode, as ω_v^- vanishes identically due to spherical symmetry. The circles denote the solutions, whose eigenfunctions are shown in Fig. 6.
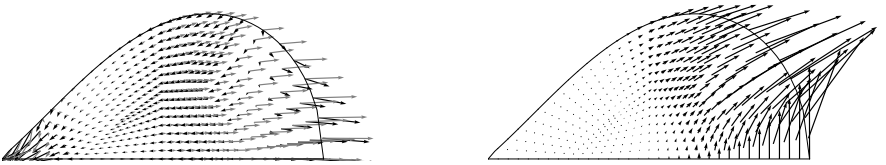

Figure 6. Eigenfunctions of the radial (left) and vertical (right) non-axisymmetric epicyclic oscillations of relativistic tori with cusp surrounding Schwarzschild black hole. In the case of the radial epicyclic mode, we show the eigenfunction of the unstable mode corresponding to merged $\omega_r^\pm$ branches. The eigenfunction is complex, the real and imaginary part of the velocity perturbation is shown by black and gray arrows, respectively. In the case of the vertical oscillations, we show the eigenfunction corresponding to v$^+$-mode. The parameters of the torus are $r_0 = 9M, \beta = \beta_{\max} = 0.452$ and $n = 3$ in both cases and correspond to the circles in Fig. 5.
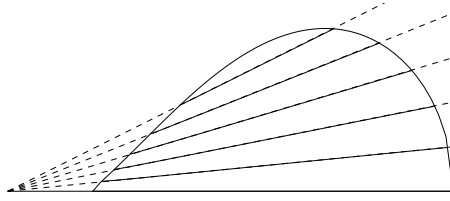
Figure 7. Eigenfunction of the nonaxisymmetric ($m = 1$) v$^-$-mode of tori surrounding Schwarzschild black hole may serve as an independent check of the accuracy of the numerical procedure. From the symmetry reasons, the eigenfunctions of this mode has to be $W_v^- = C \cot \theta$, independently of the torus thickness. The solid lines are contours of constant W_v^- in the numerical eigenfunction. The dashed lines corresponds to $\theta = $ const. The parameters of the torus are $r_0 = 9M$, $\beta = \beta_{\max} = 0.452$ and $n = 3$.

$\omega = m\Omega_0 \pm \sigma$, where σ is an eigenfrequency of the axisymmetric problem. In particular, for a given m, there are two radial (denoted as r$^\pm$) and two vertical (v$^\pm$) epicyclic modes with frequencies $\omega_r^\pm = m\Omega_0 \pm \omega_r$ and $\omega_v^\pm = m\Omega_0 \pm \omega_\theta$. We examine a behavior of all four modes with increasing torus thickness. We restrict ourselves to tori surrounding Schwarzschild black hole.

Figure 5 shows behavior of the r$^\pm$-radial modes and v$^+$-vertical mode with changing thickness parameter β for three representative radii, $r_0 = 8M$, $9M$ and $15M$. As in the axisymmetric case, the solid lines represent numerical solution of the equation (13) and dashed lines correspond to analytical approximations of Fragile et al. (2016). Examples of the corresponding eigenfunctions are shown in Fig. 6.

In the case of the radial oscillations, the numeric and analytic curves agrees well for tori of moderate thicknesses, $\beta \lesssim 0.3$. However, at higher thicknesses we observe qualitatively different type of behavior: the two branches corresponding to $\omega_r^\pm$ merge and develop a couple of overstable and damped modes. The two new modes oscillate with the same frequency (given by real parts of their eigenfrequencies), and opposite growth rates (imaginary parts). Consequently, their eigenfunctions are complex conjugated. An example of the overstable mode eigenfunction is shown in left panel of Fig. 6. The mechanism behind is related to the Papaloizou-Pringle instability and is discussed in more details in section 7.

In the case of the vertical oscillations, the behavior of the oscillation frequencies and accuracy of the analytic approximations is similar to the axisymmetric case. We show only v$^+$ oscillations in Fig. 5 as the eigenfrequencies ω_v^- vanish identically for the case of Schwarzschild black hole. This is a consequence of spherical symmetry of the spacetime. The v$^-$ oscillations in the $m = 1$ case (and by symmetry v$^+$ oscillations in the $m = -1$ case as well) can be separated out by introducing a suitably chosen tilt of the equatorial plane. These oscillations therefore correspond to neutral modes. Nevertheless, these mode may serve us as a very useful check of the accuracy of the numerical calculations. Being just a rigid infinitesimal tilt, it is possible to show that their eigenfunctions are simply given by $W_v^- = C \cot \theta$, where C is a normalization constant and θ is the meridional angle of the Schwarzschild coordinates (Blaes, 2017, unpublished). In other words, the lines of
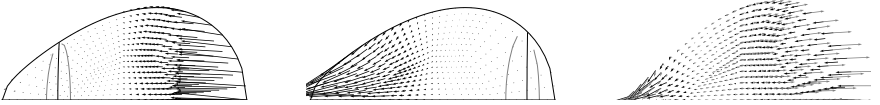
Figure 8. The eigenfunctions of the non-axisymmetric ($m = 1$) radial epicyclic modes and the mechanism of the instability. The left and middle panel show eigenfunctions of the $r^\pm$ modes in the torus of moderate thickness ($\beta = 0.6\beta_{max} = 0.27$). The right panel shows the eigenfunction of the unstable modes developed after $\omega_r^\pm$ merges and corresponds to $\beta = 0.9\beta_{max} = 0.407$. The center of the torus is located at $r_0 = 9M$. The black and gray arrows show real and imaginary parts of the velocity fields. The black solid line denote corotation radius. The inner and outer sonic radii are shown by gray curves.

constant W_v^- on the torus cross-section coincide with those of constant θ. Fig. 7 shows that the eigenfunctions W_v^- calculated using our numerical method have this property.

7   PAPALOIZOU-PRINGLE INSTABILITY

Dynamics of the $r^\pm$ non-axisymmetric modes share many common features with those of a simplified shearing sheet model of Narayan et al. (1987). In this section we apply their essential results to our problem in order to qualitative understand behavior of the non-axisymmetric radial epicyclic modes.

The left and middle panels of Fig. 8 show eigenfunctions of the r^+ and r^- modes for $r_0 = 9M$ and $\beta = 0.6\beta_{max} = 0.27$. They correspond to two distinct real eigenfrequencies on separate $\omega_r^\pm$ branches before the two modes merge (see Fig. 5, left). In each panel we also plot the lines where the local frequency of the oscillations matches the orbital velocity of the fluid Ω ('corotation radius') and the frequencies $\Omega_{1,2}$ (outer and inner 'sonic radii'). An observer moving with the fluid at these radii would measure either zero or sonic pattern speed of the oscillations. The two eigenfunctions show very different velocity patterns; while the most of the oscillations is concentrated to the outer parts of the torus in the case of the r^+, in the case of the r^- the most variable is the inner part. This behavior can be understand by exploring conditions for a wave propagation in the torus. A WKBJ analysis of equation (13) shows that the wave-like disturbances can freely propagate only outside the region limited by the sonic radii, while there is an wave-evanescent region in between. In the case of isolated $r^\pm$ modes, the oscillations are trapped in a larger region, either between the outer sonic radius and the outer boundary of the torus (the case of r^+ mode), or between the inner sonic radius and inner edge of the torus (the case of r^- mode).

According to Narayan et al. (1987), waves propagating outside or inside the corotation radius carry positive or negative conserved wave action, respectively. Therefore, the total action of the r^+ mode is positive and that of r^- mode is negative. As the torus thickness further increase, the corotation and sonic radii gradually move towards the center of the torus allowing another trapping cavity to appear on the other side of the corotation. As a consequence, a wave trapped in this cavity reduce the absolute value of the total action of

◀◀ ◀ ▶ ▶▶

the modes. At the moment when the $\omega_r^{\pm}$ branches merge, a standing wave pattern on both sides of the corotation is established and the total action of the mode vanishes, because the waves trapped in the two cavities carry exactly opposite actions. As time passes, these actions are further increased by tunneling effect through the evanescent region from one side of the corotation to another. As a result, an overstable neutral mode develops (see the right panel of Fig. 8).

8   CONCLUSIONS

This note summarizes some aspects of our ongoing study of oscillation modes of thick relativistic disks. We concentrated here only on the case of constant specific angular momentum flows. We reviewed a basic theory of stationary thick disks solutions and briefly discussed occurrence of the two possible maximal configuration – radially infinite tori and finite tori terminating by the cusps at their inner edges. We have noted that the cusp tori can be constructed only in a close vicinity of black holes; with increasing black-hole spin, a possible region reduces significantly. We also mentioned several mathematical aspects of the theory of torus oscillations and introduced the finite-element numerical method to solve the corresponding eigenvalue problem.

The main motivation for our study was to explore range of applicability of the second-order analytic approximations of Fragile et al. (2016) in terms of a torus thickness parameter β. Although Fragile et al. (2016) considered also higher-order modes (X, plus, and breathing), we have restricted ourselves to the epicyclic modes only. We have found that analytic approximation can be safely applied to the axisymmetric radial epicyclic mode almost in a whole range of possible β. Its agreement with the numerical solutions in this case is astonishing. On the other hand, a comparison of the results in the case of vertical axisymmetric oscillations is not so impressive. The analytic formula give a reasonable approximation only for $\beta \lesssim 0.1$. Behind this limit, the dependence of the eigenfrequencies on the torus thickness seems to be rather linear, in contrast to the quadratic one proposed by Fragile et al. (2016).

The situation is more complicated in the case of the non-axisymmetric modes where the numerical solution revealed an instability of the radial epicyclic modes. We have provided a qualitative description of the instability mechanism based on the general analysis of Narayan et al. (1987). As the instability occurs in a limited range of *finite* torus thicknesses, it is very unlikely that this behavior could be captured by analytic perturbation calculations based on an expansion around a slender-torus limit.

ACKNOWLEDGEMENTS

REFERENCES

Abramowicz, M., Jaroszynski, M. and Sikora, M. (1978), Relativistic, accreting disks, *Astronomy and Astrophysics*, **63**, pp. 221–224.

Abramowicz, M. A., Blaes, O. M., Horák, J., Kluzniak, W. and Rebusco, P. (2006), Epicyclic oscillations of fluid bodies: II. Strong gravity, *Classical and Quantum Gravity*, **23**, pp. 1689–1696, arXiv: `astro-ph/0511375`.

Arndt, A., Bangerth, W., Davydov, D., Heister, T., Heltari, L., Kronbichler, M., Maier, M., Pelteret, J. P., Turcksin, B. and Wells, D. (2017), The deal.II Library, Version 8.5, *Journal of Numerical Mathematics*, **25**(3), pp. 137–146.

Blaes, O. M., Arras, P. and Fragile, P. C. (2006), Oscillation modes of relativistic slender tori, *Mounthly Notices Roy.Astronom.Soc.*, **369**, pp. 1235–1252, arXiv: `astro-ph/0601379`.

Done, C., Gierliński, M. and Kubota, A. (2007), Modelling the behaviour of accretion flows in X-ray binaries. Everything you always wanted to know about accretion but were afraid to ask, *The Astronomy and Astrophysics Review*, **15**, pp. 1–66, arXiv: `0708.0148`.

Fragile, P. C., Straub, O. and Blaes, O. (2016), High-frequency and type-C QPOs from oscillating, precessing hot, thick flow, *Mounthly Notices Roy.Astronom.Soc.*, **461**, pp. 1356–1362, arXiv: `1602.08082`.

Kozlowski, M., Jaroszynski, M. and Abramowicz, M. A. (1978), The analytic theory of fluid disks orbiting the Kerr black hole, *Astronomy and Astrophysics*, **63**, pp. 209–220.

Montero, P. J., Rezzolla, L. and Yoshida, S. (2004), Oscillations of vertically integrated relativistic tori - II. Axisymmetric modes in a Kerr space-time, *Mounthly Notices Roy.Astronom.Soc.*, **354**, pp. 1040–1052, arXiv: `astro-ph/0407642`.

Narayan, R., Goldreich, P. and Goodman, J. (1987), Physics of modes in a differentially rotating system - Analysis of the shearing sheet, *Mounthly Notices Roy.Astronom.Soc.*, **228**, pp. 1–41.

Papaloizou, J. C. B. and Pringle, J. E. (1984), The dynamical stability of differentially rotating discs with constant specific angular momentum, *Mounthly Notices Roy.Astronom.Soc.*, **208**, pp. 721–750.

Rezzolla, L., Yoshida, S. and Zanotti, O. (2003), Oscillations of vertically integrated relativistic tori - I. Axisymmetric modes in a Schwarzschild space-time, *Mounthly Notices Roy.Astronom.Soc.*, **344**, pp. 978–992, arXiv: `astro-ph/0307488`.

Straub, O. and Šrámková, E. (2009), Epicyclic oscillations of non-slender fluid tori around Kerr black holes, *Classical and Quantum Gravity*, **26**(5), 055011, arXiv: `0901.1635`.

Wielgus, M., Fragile, P. C., Wang, Z. and Wilson, J. (2015), Local stability of strongly magnetized black hole tori, *Mounthly Notices Roy.Astronom.Soc.*, **447**, pp. 3593–3601, arXiv: `1412.4561`.